Journal of
Synchrotron Radiation

ISSN 0909-0495

Received 5 May 2011
Accepted 27 July 2011

Increased strontium uptake in trabecular bone of ovariectomized calcium-deficient rats treated with strontium ranelate or strontium chloride

Bernhard Pemmer,[a] Jochen G. Hofstaetter,[b,c] Florian Meirer,[d,a] Stephan Smolek,[a] Peter Wobrauschek,[a] Rolf Simon,[e] Robyn K. Fuchs,[f] Matthew R. Allen,[f] Keith W. Condon,[f] Susan Reinwald,[f] Roger J. Phipps,[g] David B. Burr,[f,h] Eleftherios P. Paschalis,[b] Klaus Klaushofer,[b] Christina Streli[a] and Paul Roschger[b]*

[a]Atominstitut, Technische Universitaet Wien, Stadionallee 2, 1020 Vienna, Austria, [b]Ludwig Boltzmann Institute of Osteology at the Hanusch Hospital of WGKK and AUVA Trauma Center Meidling, First Medical Department, Hanusch Hospital, 1140 Vienna, Austria, [c]Department of Orthopaedic Surgery, Vienna General Hospital, Medical University of Vienna, Austria, [d]MiNALab, CMM-Irst, Fondazione Bruno Kessler, Via Sommarive 18, 38123 Trento, Italy, [e]Institute for Synchrotron Radiation, Karlsruhe Institute of Technology, Campus South, 76344 Eggenstein-Leopoldshafen, Germany, [f]Department of Anatomy and Cell Biology, Indiana University School of Medicine, Indianapolis, USA, [g]Husson University School of Pharmacy, 1 College Circle, Bangor, ME 04401, USA, and [h]Department of Biomedical Engineering, Indiana University–Purdue University Indianapolis (IUPUI), Indianapolis, USA. E-mail: paul.roschger@osteologie.at

Based on clinical trials showing the efficacy to reduce vertebral and non-vertebral fractures, strontium ranelate (SrR) has been approved in several countries for the treatment of postmenopausal osteoporosis. Hence, it is of special clinical interest to elucidate how the Sr uptake is influenced by dietary Ca deficiency as well as by the formula of Sr administration, SrR *versus* strontium chloride ($SrCl_2$). Three-month-old ovariectomized rats were treated for 90 days with doses of 25 mg kg^{-1} d^{-1} and 150 mg kg^{-1} d^{-1} of SrR or $SrCl_2$ at low (0.1% Ca) or normal (1.19% Ca) Ca diet. Vertebral bone tissue was analysed by confocal synchrotron-radiation-induced micro X-ray fluorescence and by backscattered electron imaging. Principal component analysis and *k*-means clustering of the acquired elemental maps of Ca and Sr revealed that the newly formed bone exhibited the highest Sr fractions and that low Ca diet increased the Sr uptake by a factor of three to four. Furthermore, Sr uptake in bone of the $SrCl_2$-treated animals was generally lower compared with SrR. The study clearly shows that inadequate nutritional calcium intake significantly increases uptake of Sr in serum as well as in trabecular bone matrix. This indicates that nutritional calcium intake as well as serum Ca levels are important regulators of any Sr treatment.

Keywords: strontium ranelate; strontium chloride; dietary calcium; ovariectomized rats; SR μ-XRF; qBEI; elemental mapping; principal component analysis; *k*-means clustering.

1. Introduction

Strontium has been studied in the context of a possible therapeutic agent for skeletal diseases for more than half a century (Marie *et al.*, 1985; McCaslin & Janes, 1959; Shorr & Carter, 1952; Skoryna, 1981; Storey, 1962; Grynpas & Marie, 1990). Based on results of recent clinical trials showing reduced vertebral and non-vertebral fracture risk, strontium ranelate (SrR) is now approved in several countries for the treatment of postmenopausal osteoporosis (Reginster *et al.*, 2008). Studies on potential mechanisms for SrR antifracture efficacy include effects on bone microarchitecture and bone remodeling balance (Ammann *et al.*, 2007; Fuchs *et al.*, 2008*a*; Ma *et al.*, 2011) and Sr interaction with the calcium-sensing receptor of bone cells (Brennan *et al.*, 2009). Recent studies investigated Sr accumulation and storage in bone and whether Sr has an impact on the intrinsic material properties of bone (Li *et al.*, 2010; Roschger *et al.*, 2010). It should be emphasized that Sr, with its about two-fold larger atomic weight compared with Ca, interferes with the measurement of bone mineral density (BMD), which is a clinically important surrogate parameter for antifracture effectiveness. Consequently, in Sr-treated patients, changes in BMD occur not only due to changes in bone volume and/or mineral content but also due

Table 1
Sr^{2+} uptake of bone tissues analysed.

Data shown are median and range [min; max] obtained from the elemental maps performed for each bone tissue sample. N = number of maps per sample. Calcium diet: 1.19% is normal, 0.1% is deficient. Sr/(Ca + Sr): values of cluster C4 (region of highest Sr fractions) representing the newly formed bone matrix (see also Fig. 2). p-Values between the groups of single Sr/(Ca + Sr) outcomes of each bone sample. p-Values in parentheses means that the data of SrR and $SrCl_2$ samples were correspondingly pooled. none: non-treated with SrR or $SrCl_2$; ns: not significant.

Experimental data				p-Values between groups of maps			
Sample (N)	Sr^{2+} doses (mg kg^{-1} d^{-1})	Ca diet (wt%)	Sr/(Ca + Sr) (count rates)	*Versus* control	Low *versus* high Sr	Deficient *versus* normal Ca	SrR *versus* $SrCl_2$
1*c* (3)	SHAM none	1.19	0.0012 [0.0010; 0.0013]				
2*c* (4)	OVX none	1.19	0.0011 [0.0011; 0.0012]	<0.01			
3*n* (5)	SrR 8.5	1.19	0.024 [0.020; 0.024]	<0.01			ns
4*n* (4)	$SrCl_2$ 9.4	1.19	0.02148 [0.018; 0.023]	<0.05		<0.05 (<0.001)	
5*d* (3)	SrR 8.5	0.1	0.1015 [0.094; 0.109]	<0.01		<0.05 (<0.001)	ns
6*d* (4)	$SrCl_2$ 9.4	0.1	0.085 [0.081; 0.095]	<0.01	<0.05 (<0.001)		
7*n* (4)	SrR 51	1.19	0.140 [0.136; 0.153]	<0.001	<0.01 (<0.001)		<0.05
8*n* (8)	$SrCl_2$ 56	1.19	0.130 [0.105; 0.138]	<0.05	0.1 (<0.001)	0.05 (<0.001)	
9*d* (3)	SrR 51	0.1	0.4252 [0.418; 0.435]	<0.01	<0.05 (<0.001)	<0.01 (<0.001)	0.057
10*d* (4)	$SrCl_2$ 56	0.1	0.3528 [0.322; 0.378]				

to Sr uptake, which makes reliable interpretation of osteodensitometry difficult (Bärenholdt *et al.*, 2009; Blake & Fogelman, 2007; Kendler *et al.*, 2009). Bearing in mind that, in vertebrates, 99% of whole body Ca and Sr is located in bone (Dahl *et al.*, 2001), the amount incorporated is positively correlated with serum levels of Sr as numerous studies have shown (Dahl *et al.*, 2001; Fuchs *et al.*, 2008*a*; Li *et al.*, 2010; Roschger *et al.*, 2010; Boivin *et al.*, 1996; Farlay *et al.*, 2005). In addition, it was recently demonstrated that Sr is preferentially located in the new bone formed during Sr treatment and only marginally located in the pre-existing bone matrix (Fuchs *et al.*, 2008*a*; Li *et al.*, 2010; Roschger *et al.*, 2010). Sr atoms are incorporated into the crystal lattice of the bone hydroxyapatite by ionic substitution of calcium (Li *et al.*, 2010).

A recent study in ovariectomized (OVX) rats (Fuchs *et al.*, 2008*a*) determined the effects of high (150 mg kg^{-1} d^{-1}) and low (25 mg kg^{-1} d^{-1}) dose SrR on bone histomorphometric indices, mechanical properties and Sr uptake. Furthermore, the role of dietary calcium in modulating the effect of SrR on the skeleton was examined by feeding rats either a normal (1.19% Ca) or a low calcium diet (0.1% Ca). The concentration and distribution of Ca and Sr in cortical bone tissue of the tibial midshaft region was determined using a synchrotron-radiation-induced micro X-ray fluorescence (SR μ-XRF) method. Animals treated with high-dose SrR had significantly higher Sr incorporation, regardless of Ca intake. However, compared with the normal Ca diet, the low Ca diet increased the incorporation of Sr into the bone for low- and high-dose SrR groups. All animals treated with SrR had a higher Sr fraction at the periosteal bone surface (newly formed bone regions) compared with intracortical bone regions (older bone).

The aim of the present study was to expand these investigations to the administration of Sr by $SrCl_2$ as well as SrR with low and normal Ca diets. A further aim was to extend the analysis for Sr uptake and distribution into the geometrical more complex trabecular bone compartment of the vertebrae, which contains bone marrow, in contrast to tibial periosteal bone. For this purpose, an advanced state-of-the-art confocal SR μ-XRF technique was used. Quantitative backscattered electron imaging (qBEI) was employed to select regions of interest for SR μ-XRF. In addition, principal component analysis and *k*-means clustering were used to analyze the elemental maps and to separate regions with typical Sr to Ca fractions within the samples. This is the first time that such a technique of analysis of elemental maps has been applied to the study of bone tissue.

2. Methods and materials

2.1. Bone samples

We analyzed bone samples from the previously reported study (Fuchs *et al.*, 2008*a*) on Sr treatment in three-month-old OVX Sprague-Dawley rats. The animal study was approved by Indiana University's Institutional Animal Care and Use Committee. OVX rats were randomized by body mass three weeks post surgery and divided into eight different treatment regimens: low (25 mg kg^{-1} d^{-1}) and high (150 mg kg^{-1} d^{-1}) dose SrR with low (0.1% Ca) and normal (1.19% Ca) dietary Ca; low (25 mg kg^{-1} d^{-1}) and high (150 mg kg^{-1} d^{-1}) $SrCl_2$ with low (0.1% Ca) and normal (1.19% Ca) dietary Ca. The Sr^{2+} ion equivalents for SrR with the chemical formula $C_{12}H_6N_2O_8SSr_2$ (513.49 g mol^{-1}) were 8.5 mg kg^{-1} d^{-1} and 51 mg kg^{-1} d^{-1}, and for $SrCl_2$ with the chemical formula $SrCl_26(H_2O)$ (266.62 g mol^{-1}) were 9.4 mg kg^{-1} d^{-1} and 56 mg kg^{-1} d^{-1}, for the low and high Sr doses, respectively. SHAM operated and untreated OVX rats fed a normal Ca diet served as controls. Animals were treated daily for 90 d. According to previously published Sr serum level data (Fuchs *et al.*, 2008*a*) the different treatments regimes led to the following mean Sr serum levels: 22.7 and 23.3 ng ml^{-1} for untreated SHAM and OVX, 2226.7 and 293.5 ng ml^{-1} for 25 mg kg^{-1} d^{-1} SrR treatment at 0.1% and 1.19% Ca diet, respectively, 12611.1 and 1746.0 ng ml^{-1} for 150 mg kg^{-1} d^{-1} SrR treatment at 0.1% and 0.19% Ca diet, respectively. One L3 vertebra from each group was used for analysis, while all the measurements of the bone samples were performed blinded to the treatment (Table 1).

Vertebrae were fixed in 70% ethanol, dehydrated through a graded series of ethanol, and embedded undecalcified in polymethylmethacrylate (PMMA). About 5 mm-thick blocks containing a sagittal vertebral bone section were obtained using a low-speed diamond saw (Buehler Isomet, Lake Pluff, USA). The section surfaces were ground by sand paper and subsequently polished using a diamond suspension (3 and 1 μm grain size) on a precision polishing device (PM5 Logitech, Glasgow, Scotland). The sample surface was carbon coated (Agar SEM Carbon Coater, Stansted, UK) prior to qBEI and subsequent SR μ-XRF analysis.

2.2. qBEI

The intensity of electrons backscattered from the sample surface is proportional to the average atomic number of the target material. For trabecular bone tissue from the rat vertebral bodies, the weight fraction of Ca (atomic number Z = 20) predominantly influences the material contrast of the bone tissue, which is composed of an organic phase (Z = 6) and a hydroxyapatite mineral phase (Z = 14). Details of the technique can be found elsewhere (Fratzl-Zelman *et al.*, 2009; Roschger *et al.*, 1998, 2008). qBEI images the local mineral content with a spatial resolution of <1 μm. Thus, areas with high backscattered electron intensities, *i.e.* bright gray levels in the image, represent mineralized matrix with high Ca content, whereas areas with low intensities, *i.e.* dark gray levels, indicate low Ca content. The method cannot distinguish between a local increase in gray levels caused by Sr uptake (Z = 38) *versus* Ca. Hence, element-specific methods had to be used to localize and quantify the Sr uptake.

qBEI was performed in a digital scanning electron microscope (DSM 962, Zeiss, Oberkochen, Germany) equipped with a four-quadrant semiconductor backscattered electron detector. The microscope was operated at an acceleration voltage of 20 kV, the working distance kept at 15 mm, and the probe current was maintained at 110 pA. The entire trabecular bone area was imaged by qBEI using a pixel resolution of 1 μm. From these qBEI gray-scale images, areas of interest (ROI) have been selected for elemental mapping by confocal SR μ-XRF. The selection criteria were such that the ROI contained trabecular bone features with bone regions (packets) of low and light gray levels representing the coexistence of young and older bone matrix (Fig. 1).

2.3. SR μ-XRF analysis

Micro-XRF is based on the detection of characteristic X-rays induced by high-energy primary photons (Van Grieken & Markowicz, 2002). Using synchrotron radiation as exciting X-ray source, the outstanding properties of synchrotron radiation, including high photon flux, natural collimation, polarization and the possibility to select the energy of the primary photons, greatly increase the spatial resolution and detection limits (fg-range, μm-range) of the μ-XRF. In combination with confocal geometry, high-sensitive element mapping with spatial resolution in the micrometer range can be performed (Zoeger *et al.*, 2006, 2008). More details on confocal SR μ-XRF are provided elsewhere (Zoeger *et al.*, 2006, 2008; Janssens *et al.*, 2004; Kanngießer *et al.*, 2003; Vincze *et al.*, 2004; Simon *et al.*, 2007).

In the present study the confocal SR μ-XRF set-up was installed at the FLUO beamline at ANKA (Karlsruhe, Germany) (Simon *et al.*, 2003). Two polycapillary half lenses with overlapping focal spots were used. The set-up was tested with reference samples revealing a beam size of 10 μm × 10 μm and a depth resolution of 12 μm at 14.2 keV (Sr $K\alpha$). To achieve optimal excitation conditions for Sr *K*-lines, the excitation energy was adjusted to 17.7 keV by means of a W/Si multilayer monochromator. The detector was a 50 mm^2 silicon drift detector (Vortex, SII NanoTechnology, USA) connected to a digital signal processor (Saturn, XIA, USA). At a measuring time of 1 s per spectrum the sensitivity of the method was sufficient for detection of the natural Sr content of bone (about 0.1 wt%).

The scans on the sample surface were performed as area scans ranging from 300 μm × 300 μm up to 850 μm × 850 μm depending on the ROI on the sample. For each ROI, several depth scans were performed to determine the correct measurement plane. The optimal depth is where the Ca $K\alpha$ intensity of the depth scans reaches its maximum. This procedure ensures that the measurement plane is parallel to the sample surface and so all measured voxels are at the same depth within the sample. The acquired spectra were processed using the *microxrf2* software package (B. Vekemans, XMI, Universiteit Gent) installed at the beamline to generate the elemental maps. Peak deconvolution and subtraction of the spectral background was carried out with the *AXIL* (Van Espen *et al.*, 1986) module implemented in this package. The resulting maps of net intensities were normalized to counts per second and 100 mA storage ring current, and were converted to 8-bit grayscale images.

2.4. Principal component analysis and *k*-means clustering

Owing to the large number of maps (up to eight scans per sample and ten samples resulting in a total of 42 scans), an automated image data analysis technique was used to extract the typical Sr to Ca $K\alpha$-lines counts fractions of the bone areas. This method was originally established and described by Vekemans *et al.* (1997). Like all other clustering methods *k*-means clustering (KMC) allows calculation of the degree of similarity (or distance in property space) between two objects to be clustered. In the presented case the objects are pixels (index i) and their properties are either X-ray intensities derived from the spectrum of pixel i or the score values of that pixel on the equivalent principal component axes. The similarity measure between two pixels A and B can then be expressed as Euclidian distance in property space. The result of such a clustering (after principal component pre-treatment) is displayed in Fig. 2. The pre-treatment using principal component analysis (PCA) is not indispensable but allows for more rapid processing of the data set by eliminating noise and reducing dimensionality prior to the clustering (*e.g.* if more than two pixel properties, here X-ray intensities of specific

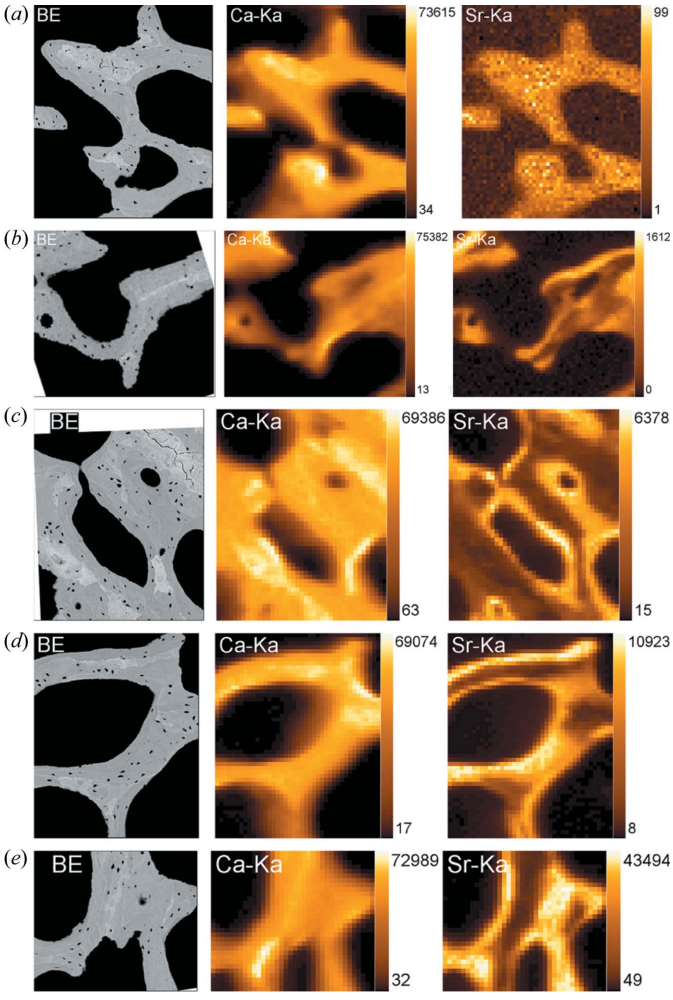

Figure 1
Examples of qBEI images and the corresponding SR μ-XRF elemental maps of calcium (Ca) and strontium (Sr) based on Ca *Kα* and Sr *Kα* fluorescence lines, respectively, from bone samples of animals untreated and treated by SrR or $SrCl_2$: (*a*) untreated, (*b*) low Sr dose at normal Ca diet, (*c*) low Sr dose at deficient Ca diet, (*d*) high Sr dose at normal Ca, and (*e*) high Sr dose at deficient Ca. The pixel size of the SR μ-XRF elemental maps is 10 μm × 10 μm with a depth resolution of 12 μm at Sr *Kα* (14.2 keV). The color-coded X-ray intensities (counts s^{-1}) are scaled from minimum to maximum. qBEI shows young bone packets (less mineralized) as darker, and older bone packets as well as residual cartilage (higher mineralized) as brighter gray levels.

elements, are investigated). The clustering algorithm could also be applied to the X-ray maps directly; however, in this case only images should be used showing high contrasts (low noise) which are appropriately scaled to each other. The approach using PCA to pre-process the data before KMC takes care of the image selection (noise removal) and scaling problem.

A number of four clusters proved to be sufficient for proper KMC results, as more than four clusters led to empty clusters in the result. PCA and KMC were performed for all samples. The classification of the clusters C1, C2, C3, C4 was performed by considering their Sr counts fraction values [Sr/(Sr + Ca)] (Fig. 2). The median and range [min; max] (Table 1) of the Sr to Ca counts fraction values of cluster C4 from the individual elemental maps per bone tissue sample was determined.

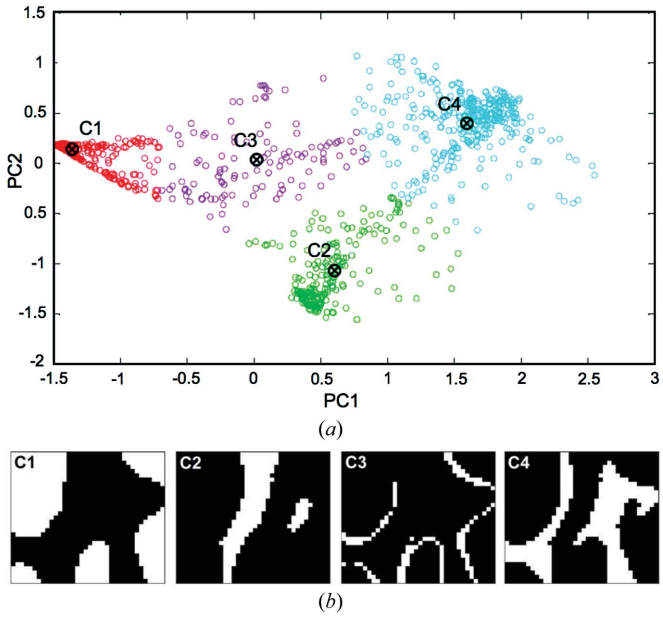

Figure 2
Example of a PCA + KMC analysis. The scan was performed on a sample (9*d* of Table 1) with high-dose SrR treatment at deficient Ca diet. (*a*) Score plot of principle components PC1 *versus* PC2 derived from a plot of Ca *versus* Sr intensities by linear transformation exhibiting a new set of mutually orthogonal axes. The PC1 axis represents the direction of constant Sr/Ca ratios. The PC2 axis represents the direction of changing Sr/Ca ratios. The KMC analysis of the PCA score plot used four clusters ($k = 4$), color-coded red, green, pink and blue; the crosses in circles are centroids of clusters C1, C2, C3, C4. The meaning of the clusters can be explained by generating binary images, where all pixels corresponding to a certain cluster are displayed in white (*b*). (*b*) Binary images produced according to the cluster data: image C1 shows the distribution of pixels clustered in C1 (red) and corresponds to the background/bone-marrow space, where both Ca and Sr concentrations are zero. Image C2 (pixels from cluster C2, green) highlights areas of old bone showing a low Sr to Ca fraction, while image C3 (pixels clustered in C3, purple) contains pixels representing the rim region of the bone. Finally, image C4, which contains all pixels of cluster C4 (cyan), displays pixels of highest Sr to Ca fraction, corresponding to areas of young bone.

Cluster C4 was the region of highest Sr counts fractions representing the newly formed bone matrix (Fig. 2). Mann-Whitney tests between the groups of single Sr/(Ca + Sr) outcomes from each bone sample were performed to determine the significance levels (*p*-values) of the differences. A value of $p < 0.05$ was considered as significant. Additionally, the significance of differences between low and high Sr doses or deficient and normal Ca content were also evaluated independently for type of administration (SrR and $SrCl_2$). In these cases the outcomes of SrR and $SrCl_2$ samples were correspondingly pooled (Table 1).

3. Results

Sr levels were measured in vertebral trabecular bone in rats treated with low- and high-dose SrR and $SrCl_2$ with normal and low Ca diet, and in untreated controls. Based on qBEI images, areas containing newly formed bone were selected for confocal SR μ-XRF. Examples of maps (Ca, Sr and corresponding qBEI) for five treatment groups are shown in Fig. 1.

Comparing the elemental maps of Sr with the corresponding qBEI images revealed that, with Sr administration, Sr was mainly incorporated into the newly formed bone matrix predominantly adjacent to the bone surface (darker gray-levels in qBEI), and was marginally incorporated into the old higher mineralized bone packets (brighter gray-levels in the qBEI images). Untreated controls (Fig. 1*a*) showed a homogeneous Sr distribution of natural Sr, with the lowest level of Sr count rates. This indicates that, with natural intake over time, Sr was associated with all the bone packets equally.

Considering the maximum of Sr count rates in the Sr maps as indicated by color-coded intensity scales (Fig. 1*a*–1*e*), bone samples from different Sr treatment regimes show Sr count rates ascending from low Sr dose with normal Ca diet followed by low Sr with low Ca diet, high Sr dose with normal Ca diet, and finally by high Sr dose with low Ca diet.

PCA and KMC of the elemental maps (Fig. 2*a*) assigned all samples consistently into the ten different treatments. The cluster (C4) with the highest Sr counts fraction Sr/(Ca + Sr) values representing the newly formed bone was used for the assignment, because it showed the largest differences between the treatment groups (Fig. 2*b*). The C4 outcomes are shown in Table 1. The increase in the Sr to Ca counts fraction with normal Ca diet was 20.8 times for low SrR doses and 121.7 times for high SrR doses compared with untreated animals. Low Ca diet additionally increased the Sr counts fraction 89 times for low SrR dose and 365 times for high SrR dose compared with normal Ca diet. In Fig. 3 the effect of low Ca diet on Sr uptake is clearly demonstrated. Further, the direct relationship between increase in Sr uptake and that of Sr serum levels can be seen.

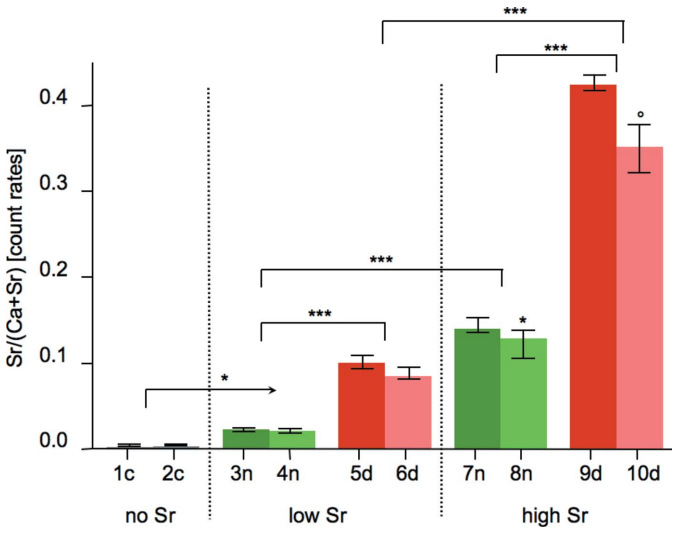

Figure 3
Influence of Ca diet on Sr uptake as quantified by cluster C4 centroid values indicated by green (normal Ca diet) and red bars (deficient Ca diet), respectively, whereby differences between SrR and $SrCl_2$ are distinguished by intense and light color. The increase in Sr uptake (height of the bars) was in parallel with the increase in Sr serum levels. For each sample, median and range (error bars) resulting from all maps recorded are indicated. Significance levels as obtained by Mann-Whitney tests: * $p < 0.05$. *** $p < 0.001$. ° $p = 0.057$.

Sr uptake in cluster C4 for low Sr dose and high Sr dose was lower for $SrCl_2$ *versus* SrR (−7.7% and −9.1%, respectively, with normal Ca diet; −20.4% and −19.8%, respectively, with low Ca diet), but differences were only partly significant (Table 1).

4. Discussion

In this analysis SR μ-XRF combined with qBEI together with PCA and KMC were used to evaluate Sr uptake into bone with different levels of Sr intake and dietary Ca intake. Analysis of the Sr to Ca fractions showed that Sr uptake in newly formed bone increases with increasing Sr dose. Low dietary Ca further elevated Sr uptake. Sr uptake in bone was slightly higher with SrR compared with $SrCl_2$ even though the Sr^{2+} equivalent in $SrCl_2$ was 10% higher than in SrR.

This is the first time that PCA and KMC have been applied to elemental maps from bone tissue to identify regions of characteristic elemental fractions. An advantage of this method is that it is mathematically objective and cannot be biased by interaction with the observer. Also the observer needs no specialized knowledge on the microscopic appearance of the elemental maps. As a result this procedure is fast, can handle a large number of maps, and can be expanded to investigate relations among more than two elements. The present analysis of the bone tissue regions with a maximum in Sr to Ca counts fraction consistently and correctly identified tissue from non-treated and from all animals treated differently with the eight combinations of Sr treatment and dietary Ca.

4.1. Ca diet *versus* Sr uptake

Low Ca significantly increased (three to four times, Table 1) the Sr to Ca counts fraction in the C4 cluster identified by qBEI imaging as newly formed bone, *i.e.* regions with low Ca content predominantly at the bone surface. In this context it is interesting how the serum levels were influenced by dietary Ca, because the serum level of Sr determines how much Sr is incorporated in the HA lattice during bone formation (Li *et al.*, 2010; Roschger *et al.*, 2010). As previously reported (Fuchs *et al.*, 2008*a*), these rats treated with 25 or 150 mg kg^{-1} d^{-1} of SrR and fed the low calcium diet (0.1% Ca) showed increases of more than seven times in serum Sr levels compared with rats fed the normal calcium diet (1.19% Ca). Such an effect of nutritional Ca deficiency might be of importance concerning safety issues of Sr treatment in patients with osteoporosis. Normal serum Ca levels, and adequate Ca and vitamin D intake, must be a prerequisite of any osteoporosis treatment. Low serum Ca levels would result in higher uptake of Sr, which can induce osteomalacia and mineralization defects (Storey, 1962; Omdahl & DeLuca, 1971; Sobel *et al.*, 1935).

4.2. SrR *versus* $SrCl_2$

We also compared Sr uptake in bone with administration of two different forms of Sr (SrR and $SrCl_2$). At both Sr^{2+} doses, low and high, the Sr uptake in the new bone matrix was higher

with SrR compared with $SrCl_2$, even though the Sr^{2+} equivalent with $SrCl_2$ was 10% higher than with SrR. For the normal Ca diet it was about 8% higher, while for the low Ca diet it was 20% higher. The results suggest that, when Sr treatment occurs at normal dietary Ca levels, SrR promotes greater uptake to bone compared with $SrCl_2$. However, care has to be taken for adequate Ca serum levels, because SrR might deliver too much Sr into the serum in the case of Ca deficiency.

4.3. Limitations

The study was designed as a pilot study for testing the sensitivity to detect spatially resolved Sr in bone after different Sr treatment regimes using a special confocal SR μ-XRF set-up. For this purpose we analyzed just one vertebral bone sample per group from ten groups; two from untreated animals (SHAM and OVX) and eight from animals of different treatment regimens (low and high Sr as SrR or $SrCl_2$ combined with normal or low dietary Ca). However, the consistency in relationship between sample outcome and treatment regime, as well as agreement with the previous analysis of the tibial/periosteal bone ($n = 10$ per group) (Fuchs *et al.*, 2008*a*), suggests that the one tissue/group analyzed in this study was representative of its treatment group. Although several numerical differences were large, many were not statistically significant. This is likely to be due to the limited number of scans per bone tissue (in majority three to four scans).

Another limitation is that the reported Sr and Ca concentrations are not given in absolute values (wt%), but always in fractions of Sr to Ca X-ray peak count rates. Unfortunately, there are no suitable reference standards for this novel experimental set-up that would have allowed calculation of absolute Sr and Ca concentrations from the X-ray count rates. Differences in sensitivity of the system to detect Ca and Sr, and differences in matrix effects between Ca $K\alpha$ and Sr $K\alpha$ X-rays make it difficult to generate suitable reference standards.

Sr serum concentrations in this study were lower or encompassed levels (12611 ng ml^{-1}, or 185 μmol L^{-1}) comparable with those produced by SrR treatment of postmenopausal osteoporosis (10560 ng ml^{-1}, or 120.4 μmol L^{-1}) (Roschger *et al.*, 2010; Fuchs *et al.*, 2008*b*). In this human study an atomic fraction for Sr to Ca of 5% was found (Roschger *et al.*, 2010; Li *et al.*, 2010), but extrapolation from animals to humans and *vice versa* should be made with caution.

5. Conclusions

In conclusion, dietary and serum levels of Ca are important determinants of serum Sr levels and Sr uptake into bone with SrR treatment for osteoporosis. To avoid higher uptake rates of Sr and improve safety in patients being treated with SrR, adequate Ca and vitamin D intake is essential.

This work was supported by the European Community Research Infrastructure Action under the FP6 'Structuring the European Research Area' ['Integrating Activity on Synchrotron and Free Electron Laser Science' (IA-SFS) RII3-CT-2004-506008], by the AUVA (Austrian Workers' Compensation Board), the WGKK (Vienna Health Insurance Fund), and a research grant from the Alliance for Better Bone Health. Further we thank G. Dinst, S. Thon, Ph. Messmer and D. Gabriel for careful sample preparations, and qBEI and EDX measurements.

References

Ammann, P., Badoud, I., Barraud, S., Dayer, R. & Rizzoli, R. (2007). *J. Bone Miner. Res.* **22**, 1419–1425.
Bärenholdt, O., Kolthoff, N. & Nielsen, S. P. (2009). *Bone*, **45**, 200–206.
Blake, G. M. & Fogelman, I. (2007). *J. Clin. Densitom.* **10**, 259–265.
Boivin, G., Deloffre, P., Perrat, B., Panczer, G., Boudeulle, M., Mauras, Y., Allain, P., Tsouderos, Y. & Meunier, P. J. (1996). *J. Bone Miner. Res.* **11**, 1302–1311.
Brennan, T. C., Rybchyn, M. S., Green, W., Atwa, S., Conigrave, A. D. & Mason, R. S. (2009). *Br. J. Pharmacol.* **157**, 1291–1300.
Dahl, S. G., Allain, P., Marie, P. J., Mauras, Y., Boivin, G., Ammann, P., Tsouderos, Y., Delmas, P. D. & Christiansen, C. (2001). *Bone*, **28**, 446–453.
Farlay, D., Boivin, G., Panczer, G., Lalande, A. & Meunier, P. J. (2005). *J. Bone Miner. Res.* **20**, 1569–1578.
Fratzl-Zelman, N., Roschger, P., Gourrier, A., Weber, M., Misof, B. M., Loveridge, N., Reeve, J., Klaushofer, K. & Fratzl, P. (2009). *Calcif. Tissue Intl*, **85**, 335–343.
Fuchs, R. K., Allen, M. R., Condon, K. W., Reinwald, S., Miller, L. M., McClenathan, D., Keck, B., Phipps, R. J. & Burr, D. B. (2008*a*). *Osteoporosis Intl*, **19**, 1331–1341.
Fuchs, R. K., Allen, M. R., Condon, K. W., Reinwald, S., Miller, L. M., McClenathan, D., Keck, B., Phipps, R. J. & Burr, D. B. (2008*b*). *Osteoporosis Intl*, **19**, 1815–1817.
Grynpas, M. D. & Marie, P. J. (1990). *Bone*, **11**, 313–319.
Janssens, K., Proost, K. & Falkenberg, G. (2004). *Spectrochim. Acta B*, **59**, 1637–1645.
Kanngießer, B., Malzer, W. & Reiche, I. (2003). *Nucl. Instrum. Methods Phys. Res. B*, **211**, 259–264.
Kendler, D. L., Adachi, J. D., Josse, R. G. & Slosman, D. O. (2009). *Osteoporosis Intl*, **20**, 1101–1106.
Li, C., Paris, O., Siegel, S., Roschger, P., Paschalis, E. P., Klaushofer, K. & Fratzl, P. (2010). *J. Bone Miner. Res.* **25**, 968–975.
Ma, Y. L., Zeng, Q. Q., Porras, L. L., Harvey, A., Moore, T. L., Shelbourn, T. L., Dalsky, G. P., Wronski, T. J., Aguirre, J. I., Bryant, H. U. & Sato, M. (2011). *Endocrinology*, **152**, 1767–1778.
McCaslin, F. & Janes, J. (1959). *Proc. Mayo Clin.* **34**, 329–334.
Marie, P. J., Garba, M. T., Hott, M. & Miravet, L. (1985). *Miner. Electrolyte Metab.* **11**, 5–13.
Omdahl, J. L. & DeLuca, H. F. (1971). *Science*, **174**, 949–951.
Reginster, J. Y., Felsenberg, D., Boonen, S., Diez-Perez, A., Rizzoli, R., Brandi, M. L., Spector, T. D., Brixen, K., Goemaere, S., Cormier, C., Balogh, A., Delmas, P. D. & Meunier, P. J. (2008). *Arthritis Rheum.* **58**, 1687–1695.
Roschger, P., Fratzl, P., Eschberger, J. & Klaushofer, K. (1998). *Bone*, **23**, 319–326.
Roschger, P., Manjubala, I., Zoeger, N., Meirer, F., Simon, R., Li, C., Fratzl-Zelman, N., Misof, B. M., Paschalis, E. P., Streli, C., Fratzl, P. & Klaushofer, K. (2010). *J. Bone Miner. Res.* **25**, 891–900.
Roschger, P., Paschalis, E. P., Fratzl, P. & Klaushofer, K. (2008). *Bone*, **42**, 456–466.
Shorr, E. & Carter, A. C. (1952). *Bull. Hosp. Joint Dis.* **13**, 59–66.
Simon, R., Buth, G. & Hagelstein, M. (2003). *Nucl. Instrum. Methods Phys. Res. B*, **199**, 554–558.
Simon, R., Kerdpin, U., Friedrich, F., Faubel, W., Weidler, P. G. & Nüesch, R. (2007). *Adv. X-ray Anal.* **50**, 64–70.

Skoryna, S. C. (1981). *Can. Med. Assoc. J.* **125**, 703–712.
Sobel, A. E., Cohen, J. & Kramer, B. (1935). *Biochem. J.* **29**, 2640–2645.
Storey, E. (1962). *J. Bone Joint Surg. Br.* **44**B, 194–208.
Van Espen, P., Janssens, K. & Nobels, J. (1986). *Chemometr. Intell. Lab. Syst.* **1**, 109–114.
Van Grieken, R. & Markowicz, A. (2002). *Handbook of X-ray Spectrometry*, 2nd ed. New York: Marcel Dekker.
Vekemans, B., Janssens, K., Vincze, L., Aerts, A., Adams, F. & Hertogen, J. (1997). *X-ray Spectrom.* **26**, 333–346.
Vincze, L., Vekemans, B., Brenker, F. E., Falkenberg, G., Rickers, K., Somogyi, A., Kersten, M. & Adams, F. (2004). *Anal. Chem.* **76**, 6786–6791.
Zoeger, N., Roschger, P., Hofstaetter, J. G., Jokubonis, C., Pepponi, G., Falkenberg, G., Fratzl, P., Berzlanovich, A., Osterode, W., Streli, C. & Wobrauschek, P. (2006). *Osteoarthritis Cartilage*, **14**, 906–913.
Zoeger, N., Streli, C., Wobrauschek, P., Jokubonis, C., Pepponi, G., Roschger, P., Hofstaetter, J., Berzianovich, A., Wegrzynek, D., Chinea-Cano, E., Markowicz, A., Simon, R. & Falkenberg, G. (2008). *X-ray Spectrom.* **37**, 3–11.